

Magnetic penetration-depth measurements of a suppressed superfluid density of superconducting $\text{Ca}_{0.5}\text{Na}_{0.5}\text{Fe}_2\text{As}_2$ single crystals by proton irradiation

Jecheon Kim,^{1,*} N. Haberkorn,¹ M. J. Graf,¹ I. Usov,¹ F. Ronning,¹ L. Civale,¹
E. Nazaretski,² G. F. Chen,³ W. Yu,³ J. D. Thompson,¹ and R. Movshovich¹

¹*Los Alamos National Laboratory, Los Alamos, NM 87545*

²*Brookhaven National Laboratory, Upton, NY 11973*

³*Department of Physics, Renmin University of China, Beijing, 100872, China*

(Dated: October 1, 2012)

We report on the dramatic effect of random point defects, produced by proton irradiation, on the superfluid density ρ_s in superconducting $\text{Ca}_{0.5}\text{Na}_{0.5}\text{Fe}_2\text{As}_2$ single crystals. The magnitude of the suppression is inferred from measurements of the temperature-dependent magnetic penetration depth $\lambda(T)$ using magnetic force microscopy. Our findings indicate that a radiation dose of $2 \times 10^{16} \text{ cm}^{-2}$ produced by 3 MeV protons results in a reduction of the superconducting critical temperature T_c by approximately 10%. In contrast, $\rho_s(0)$ is suppressed by approximately 60%. This break-down of the Abrikosov-Gorkov theory may be explained by the so-called “Swiss cheese model”, which accounts for the spatial suppression of the order parameter near point defects similar to holes in Swiss cheese. Both the slope of the upper critical field and the penetration depth $\lambda(T/T_c)/\lambda(0)$ exhibit similar temperature dependences before and after irradiation. This may be due to a combination of the highly disordered nature of $\text{Ca}_{0.5}\text{Na}_{0.5}\text{Fe}_2\text{As}_2$ with large intraband and simultaneous interband scattering as well as the s^\pm -wave nature of short coherence length superconductivity.

I. INTRODUCTION

Proximity of the superconducting and magnetic states in iron-based superconductors has stimulated extensive studies of the gap nature,^{1–3} order-parameter symmetry,^{4–6} and the pairing mechanisms in these materials.⁷ The response of the superconducting condensate to impurities is sensitive to the symmetry of the superconducting state, and their influence has been widely investigated to gain better understanding of the nature of the order parameter in both low- and high-temperature unconventional superconductors.^{8–12}

The Abrikosov-Gor’kov (AG) theory¹³ explains the effects of impurities in the low- T_c superconductors, where a large superconducting coherence length ξ effectively averages the suppression of order parameter at the impurity sites over many impurities, leading to a uniformly suppressed order parameter. However, the AG theory breaks down when applied to the effect of disorder on superconducting properties in the cuprates superconductors,¹⁰ where ξ is short and comparable to the average spacing between disorder centers. The order parameter is therefore suppressed locally at the impurity site and has a chance to recover between impurities. The influence of disorder on the superfluid density ρ_s in cuprates is well described by the so called “Swiss cheese” model, which considers spatial dependence of the order parameter and its strong suppression near defects.^{14–20} In iron-based systems, where superconductivity exhibits both s -wave characteristics and a small coherence length, the situation is between the low-temperature and high-temperature superconductors. Consequently these systems pose an intriguing question of how the effect of disorder on T_c and the superfluid density in these compounds compares to that in conventional BCS supercon-

ductors and cuprates.¹²

Recently, two irradiation experiments on Co-doped BaFe_2As_2 (Co-122) were performed to study the influence of disorder.^{11,12} The temperature-dependent penetration depth measurements suggested an s^\pm state, with strong nonmagnetic scattering in the unitary limit,¹¹ whereas transport measurements showed an s^{++} state with weak scattering in the Born limit.¹² Both experiments showed a relatively small suppression of T_c caused by nonmagnetic impurities induced by irradiation; these findings are consistent with an s^{++} state, since superconductivity with a sign changing order parameter is quite sensitive to nonmagnetic impurities.^{21–23} Reports in several iron-arsenide systems by different experimental techniques are consistent with theoretical predictions of s wave, potentially nodal s -wave or sign reversing s -wave.^{5,7}

In this work we investigate the influence of random point defects introduced by proton irradiation on $\lambda(T)$ in $\text{Ca}_{0.5}\text{Na}_{0.5}\text{Fe}_2\text{As}_2$ (CNFA) single crystals. We use the magnetic force microscopy (MFM) technique to determine absolute values of $\lambda(T)$.^{24–28} The CNFA single crystals, showing homogeneity, have been grown with a self-flux technique. Details of the sample preparation and characterization can be found elsewhere.²⁹

II. EXPERIMENT

The 3 MeV protons are known to produce between one and a few tens of atomic displacements,³⁰ creating random point defects as well as nanoclusters with typical dimensions of few nanometers. The CNFA sample was irradiated with the total proton dose of $2 \times 10^{16} \text{ cm}^{-2}$, which corresponds to an average distance (d) between defects of 2.8 nm.³¹ The sample was cleaved, and its thickness

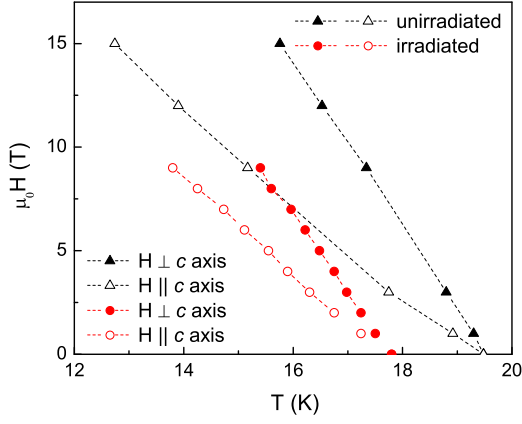


FIG. 1: (color online) Temperature dependent H_{c2} along the c axis and within the ab plane in unirradiated $\text{Ca}_{0.5}\text{Na}_{0.5}\text{Fe}_2\text{As}_2$ (black triangles), taken from Ref. 24, and proton irradiated $\text{Ca}_{0.5}\text{Na}_{0.5}\text{Fe}_2\text{As}_2$ (red circles).

measured to be around $28 \mu\text{m}$, which is smaller than the penetration range of $40 \mu\text{m}$ for the 3 MeV proton beam. Electrical resistivity in both unirradiated and irradiated samples were measured using a standard four-probe technique. The sample was mounted in a rotatable probe and measurements were performed in magnetic fields varying between 0 and 9 T. MFM measurements described here were performed in a home-built low-temperature MFM apparatus.³² Three samples, CNFA, irradiated CNFA (ICNFA), and a Nb reference film were loaded and investigated in a comparative experiment within a single cool-down. The magnetic stray field calibration was performed by imaging vortices in a Nb reference as a function of applied magnetic field.²⁴ Measurements of λ were performed using the Meissner response technique.^{24–26} The Meissner response curves were first measured as a function of the tip-sample separation in the Nb reference with known $\lambda(T)$. Subsequently, the cantilever was moved to a sample of interest and the Meissner response curves were acquired. Direct comparison of measured curves yields the absolute value of λ in a sample under investigation. Details of experimental technique are described elsewhere.^{24–26}

The reference Nb thin film ($T_c \approx 8.8 \text{ K}$) has a thickness of 300 nm and was grown by electron beam deposition. The T_c of CNFA from transport measurements is 19.4 K and that of ICNFA is 17.8 K. The width of the superconducting transition did not change after irradiation. No upturn in resistivity was observed at low temperatures, indicating that irradiation by protons results in the formation of nonmagnetic point-like scattering centers.³³ The MFM measurements were performed using a high-resolution Nanosensors cantilever³⁴ that was polarized along the tip axis in a 3 T magnetic field. Both Nb and CNFA samples were zero-field cooled for Meissner experiments; a magnetic field of a few Oe was applied above T_c , followed by cooling for vortex imaging experiments.

III. RESULTS

A. $H_{c2}(T)$ measurements

Figure 1 shows the upper critical field $H_{c2}(T)$ with $\mathbf{H} \parallel c$ and $\mathbf{H} \perp c$ (within the ab plane) for CNFA and ICNFA. $H_{c2}(T)$ is linear in both samples and for both directions, with average slopes of $\beta^{ab} = -\frac{\partial H_{c2}^{ab}}{\partial T}|_{T_c} = 4 \text{ T/K}$ and $\beta^c = -\frac{\partial H_{c2}^c}{\partial T}|_{T_c} = 2.2 \text{ T/K}$ for CNFA, and $\beta^{ab} = -\frac{\partial H_{c2}^{ab}}{\partial T}|_{T_c} = 3.8 \text{ T/K}$ and $\beta^c = -\frac{\partial H_{c2}^c}{\partial T}|_{T_c} = 2.3 \text{ T/K}$ for ICNFA. A modest superconducting anisotropy parameter $\gamma = \frac{\beta^{ab}}{\beta^c} = 1.85 - 1.65$ for both CNFA and ICNFA samples points toward a three-dimensional behavior. The superconducting coherence length ξ can be expressed in the Ginzburg-Landau region as $\xi_{GL}(T) \approx \xi_0/\sqrt{1 - T/T_c}$. In the case of a one-band model or two weakly coupled bands with similar Fermi surface properties and pairing interactions the zero-temperature in-plane coherence length ξ_0^{ab} and out-of-plane coherence length ξ_0^c are given by the slope of the upper critical field:^{29,35} $(\xi_0^{ab})^2 \approx \Phi_0/2\pi T_c \beta^c$ and $(\xi_0^c)^2 \approx \Phi_0/2\pi T_c \beta^{ab}$. We obtain the zero-temperature Ginzburg-Landau values of $\xi_{CNFA}^{ab}(0) = 2.8 \text{ nm}$ and $\xi_{ICNFA}^{ab}(0) = 2.8 \text{ nm}$, which are similar in magnitude to the short-coherence length cuprate and PuCoGa_5 superconductors. Within our measurement uncertainty no appreciable change of the coherence length took place after irradiation, although T_c is suppressed by 10%.

B. $\lambda(T)$ measurements

Prior to measurements of the absolute values of $\lambda(T)$, vortex images were obtained under the same experimental conditions for all samples. These measurements yield information about homogeneity of CNFA and ICNFA samples on a submicron scale ($\sim 100 \text{ nm}$). The well-formed single vortices in Nb and CNFA suggest the homogeneity of the sample; however, the irregular shape of single vortex in ICNFA (elongated vortex in the diagonal direction of the image) suggests the presence of inhomogeneity in the superfluid density on a sub-micron scale, which may be related to impurities introduced from irradiation. We employed the following imaging procedure: First, a single vortex in the Nb sample was obtained at 4 K after the stray field calibration of the MFM system.²⁴ Second, the MFM tip was moved on to CNFA and a single vortex image obtained, and third, a single vortex image was obtained after the tip was moved on to ICNFA as shown in Figs. 2(a), (b), and (c). The line profile for each of the single vortices is shown in Fig. 2(d). The intensity of the vortex center in different samples correlates with the magnitude of λ , since all images were taken under the same conditions and with the same tip. Lower intensity corresponds to a larger λ ; therefore, λ in ICNFA is much larger than that in the Nb reference. In

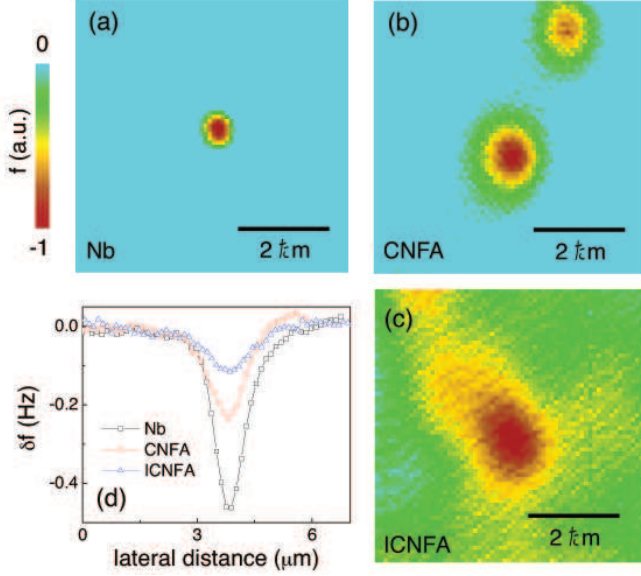


FIG. 2: (color online) Single vortex images in (a) the Nb reference, (b) the unirradiated $\text{Ca}_{0.5}\text{Na}_{0.5}\text{Fe}_2\text{As}_2$, and (c) the irradiated $\text{Ca}_{0.5}\text{Na}_{0.5}\text{Fe}_2\text{As}_2$. (d) Comparison of single vortex profiles obtained from (a), (b), and (c). All images were obtained under the same experimental conditions in a single-cool down with the tip lift height of 300 nm at 4 K. The color scale bar refers to (a)-(c).

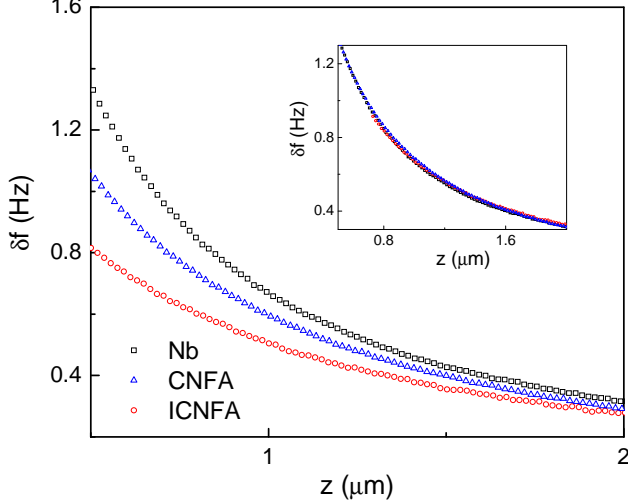


FIG. 3: (color online) Meissner response curves obtained from (a) the Nb reference (blue diamonds), (b) the unirradiated $\text{Ca}_{0.5}\text{Na}_{0.5}\text{Fe}_2\text{As}_2$ (green diamonds), and (c) the irradiated $\text{Ca}_{0.5}\text{Na}_{0.5}\text{Fe}_2\text{As}_2$ (red diamonds) at 4 K. The different slopes of the Meissner curves obtained from each sample indicate a systematic change of λ . The inset: The Meissner curves for the unirradiated and irradiated samples are shifted along the horizontal axis to overlay the Meissner curve for the reference Nb sample. The difference of the penetration depths $\Delta\lambda$ can be obtained from the values of the shift.

addition, the magnitude of λ among the superconducting samples can be inferred from the relative size of a single vortex: The larger the size, the larger is λ . Therefore, λ in ICNFA, showing the largest vortex size, is the biggest among them.

To extract absolute values of λ in ICNFA we performed the Meissner response measurements as described above. The Meissner curves as a function of the tip-sample separation were obtained in all three samples, Nb, CNFA, and ICNFA (see Fig. 3). The decay rate of the frequency shift δf as a function of the tip-sample separation z provides the relative magnitude of λ , *i.e.*, the higher the rate $d(\delta f)/dz$ the larger the λ . In bulk and thick films, the Meissner response force obeys a universal power-law dependence with tip-to-sample distance.^{27,28} The force is given by $F_{\text{Meissner}} = A \times f(\lambda + z)$, where z is the tip-to-sample distance, A is a pre-factor containing information about the geometry of the magnetic tip, and $f(z) \sim 1/z^3$. By shifting the $f^{\text{ICNFA}}(z)$ data with respect to distance in order to overlay it with the $f^{\text{Nb}}(z)$ curve, one can obtain the absolute values of $\lambda_{\text{ICNFA}}(T) = \lambda_{\text{Nb}}(T) + \Delta\lambda(T)$, where $\Delta\lambda(T)$ is the magnitude of the shift. The shift $\Delta\lambda$ between the Nb and ICNFA data equals 320 nm, resulting in $\lambda_{\text{ICNFA}}(0) = \lambda_{\text{Nb}}(0) + \Delta\lambda(0) = 110 \text{ nm} + 320 \text{ nm} = 430 \text{ nm}$. Using the same procedure we also obtained $\lambda_{\text{CNFA}}(0) = \lambda_{\text{Nb}}(0) + \Delta\lambda(0) = 110 \text{ nm} + 150 \text{ nm} = 260 \text{ nm}$. Our experimental error is around 10% and depends on the magnitude of λ and the system noise level. A key result of this work is that the $\lambda(0)$ values before and after irradiation differ significantly. This is in stark contrast to both the coherence length ξ , which shows little change after irradiation, as well as the small suppression in T_c of 10%. The Meissner force MFM measurements of the ICNFA sample were performed after cleaving followed by irradiation. The ICNFA sample was remeasured after polishing. Both measurements showed the same λ within experimental uncertainty. This indicates that irradiation does not noticeably affect sample quality. Therefore we can neglect the degradation of the sample surface for Meissner screening currents. It should be noted that our parameter free method of using the Nb reference sample is based on the assumption of a universal scaling function $F(z)$ for the Meissner force. This approach is valid for type-II superconductors, where the electromagnetic response is local, *i.e.*, $\kappa = \lambda/\xi \gg 1$. Here we neglected higher order corrections in $1/\kappa$. Our Nb film has $\kappa = \lambda/\xi = 110\text{nm}/10\text{nm} \approx 10$. The large κ value in Nb allows direct comparison of Meissner responses between the Nb reference and CNFA, which results in good agreement by overlaying the Meissner curves, shown as insets in Fig. 3 and Figs. 4(a)-(b). Our novel method of using a reference sample is justified a posteriori because the Meissner curves would not overlay with one another just by shifting them.

The temperature-dependent Meissner response curves measured in both CNFA and ICNFA samples are shown in Figs. 4(a) and (b). The gradual variation of the Meiss-

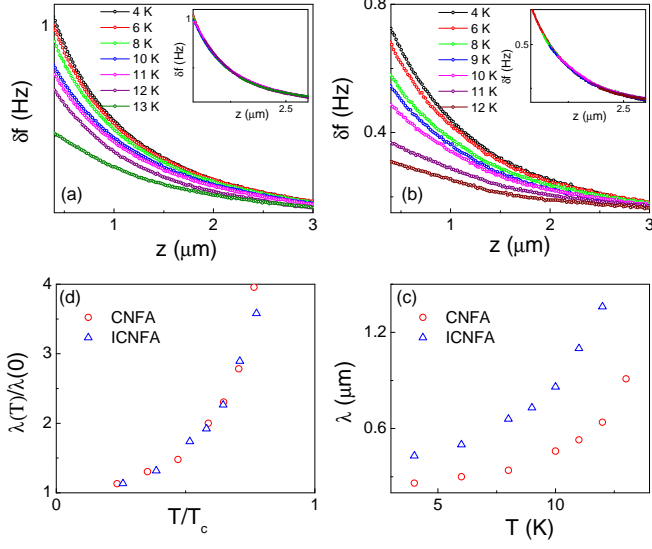


FIG. 4: (color online) Temperature dependent Meissner curves for (a) the unirradiated $\text{Ca}_{0.5}\text{Na}_{0.5}\text{Fe}_2\text{As}_2$ and (b) the irradiated $\text{Ca}_{0.5}\text{Na}_{0.5}\text{Fe}_2\text{As}_2$ samples. Insets in (a) and (b) show overlaid temperature dependent Meissner curves at 4 K, validating our procedure for extracting $\lambda(T)$. (c) Temperature dependent $\lambda(T)$ in both unirradiated and irradiated $\text{Ca}_{0.5}\text{Na}_{0.5}\text{Fe}_2\text{As}_2$ samples determined from (a) and (b). (d) $\lambda(T)$ from (c) normalized by the $T = 0$ value as a function of the normalized temperature.

ner curves as a function of temperature indicates a systematic change of $\lambda(T)$. The insets in (a) and (b) show the Meissner curves obtained at different temperatures but shifted to lie on top of the Meissner curve taken at $T = 4$ K; the curves overlay each other very well. The shift value for a given T to $T = 4$ K along the horizontal axis allows one to calculate $\lambda(T)$ at T . The resulting $\lambda(T)$ and normalized $\lambda(T)/\lambda(0)$ in both samples are shown in Figs. 4(c) and (d), respectively. Results indicate that $\lambda(T)$ increases after proton irradiation; however, the dependence of $\lambda(T)/\lambda(0)$ on the normalized temperature T/T_c is the same for both samples within our experimental uncertainty. The penetration depth exhibits the typical power-law behavior $\Delta\lambda(T)/\lambda(0) \sim T^n$ with $n \approx 2$ reported previously for doped iron-arsenide superconductors.³

IV. DISCUSSION

The radiation dose of $2 \times 10^{16} \text{ cm}^{-2}$ produced by 3 MeV protons in a $\text{Ca}_{0.5}\text{Na}_{0.5}\text{Fe}_2\text{As}_2$ sample causes the suppression of the superfluid density $\rho_s(0) \approx 1/\lambda^2(0)$ by about 60% whereas T_c is only suppressed by 10%. We plot the value of the normalized $\rho_s(0)$ for ICNFA as a solid circle in the Uemura plot³⁶ of disordered superconductors in Fig. 5, as well as theoretical results of one-band AG for d-wave pairing (solid line) and two-band AG cal-

culations for s^\pm pairing (red open circles).²² Also shown are the BdG (Bogoliubov-de Gennes) calculations for d -wave pairing (red hatched circles), a Swiss cheese model far from the AG theory.³⁷ Our result bears similarity to the data for self-irradiated PuCoGa_5 ³⁸ and He-irradiated YBCO high-temperature superconductor, showing that T_c is strongly immune to disorder relative to $\rho_s(0)$,^{39,40} contrary to the conventional AG theory for d -wave pairing. By analogy we argue that the break-down of the AG theory is accounted for by the Swiss cheese model within the BdG lattice theory of short-coherence length superconductors,³⁷ which shows an abrupt suppression of the order parameter near point defects. This model describes the spatial dependence of the local density of states and the order parameter in the vicinity (within a few lattice constants) of a point-like nonmagnetic impurity in the strong scattering limit, similar to holes in Swiss cheese. Franz and coworkers⁴¹ also reported the break down of the AG theory and strong suppression of $\rho_s(0)$ for d -wave pairing. The effect is stronger in samples with small ξ/a_0 ratio (a_0 is the lattice constant). In the opposite limit, the AG theory is valid and the order parameter is then suppressed uniformly in the entire sample because $\xi \gg a_0, d$, with d the average distance between impurities. In our sample the ratio of ξ_0/a_0 is approximately 7, $\xi \approx 2.8 \text{ nm}$ and d is about 2.8 nm, justifying the Swiss cheese scenario.

It is worth noting that the T dependence of $\lambda(T)$ remains the same after irradiation as shown in Fig. 4 (d), while it changes in cuprates.^{42–44} This discrepancy may result from the nature of the multiband s -wave pairing as well as the highly disordered nature of CNFA on the Ca/Na sites which lie above and below the iron layer. The fact that the temperature behavior of $\lambda(T)$ is robust after irradiation may be ascribed to large intraband scattering with s^\pm pairing and that the system itself is already in the “dirty” limit prior to irradiation, consistent with its short coherence length and power-law dependence of $\lambda(T)$. Additional disorder (mostly in the iron layer) by proton irradiation therefore has little impact on the temperature behavior of $\lambda(T)$, while added interband scattering is detrimental to (increases) the absolute magnitude of $\lambda(0)$.

The pair-breaking effect due to nonmagnetic scattering in the AG theory can be quantitatively analyzed using the normalized scattering rate in conjunction with λ given by: $g^\lambda = \hbar\Delta\rho_0/(2\pi k_B T_{c0} \mu_0 \lambda_0^2)$, where $\Delta\rho_0$ is residual resistivity change induced by irradiation, $\Delta\rho_0 = \rho_0^{\text{irr}} - \rho_0^{\text{unirr}}$, T_{c0} is the critical temperature before irradiation, and λ_0 is the penetration depth of the unirradiated sample.¹² The parameter g^λ and T_{c0} are expressed as $\ln(T_{c0}/T_c) = \psi(1/2 + g^\lambda T_{c0}/(2T_c)) - \psi(1/2)$, where $\psi(x)$ is the digamma function, based on the s^\pm scenario.⁴⁵ This pair-breaking result for T_c is similar to that for conventional s -wave with magnetic impurities or d -wave with nonmagnetic impurities. Here the critical scattering rate parameter, where superconductivity vanishes, is $g = g^\pm \approx 0.28$ in the s^\pm pairing state. The

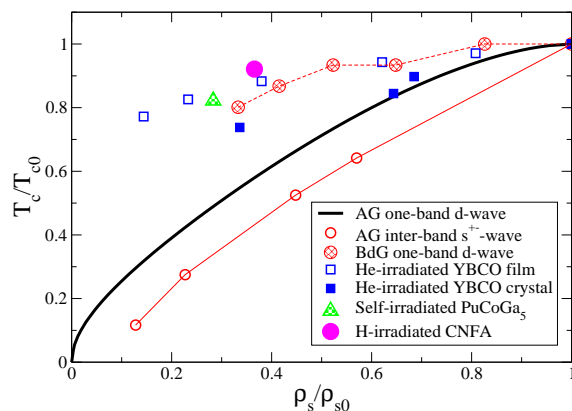


FIG. 5: (online color) Uemura plot of the superfluid density in disordered short coherence length superconductors. T_{c0} and ρ_{s0} are values obtained from a pristine crystal; T_c and ρ_s are those measured after irradiation. The solid circle represents the proton irradiated CNFA obtained in this work. For comparison we plot results of the one-band AG and BdG (Swiss cheese) calculations³⁷ for d -wave pairing, two-band AG s^\pm -wave calculations²², and experimental results for self-irradiated PuCoGa₅³⁸ and helium irradiated YBCO samples.^{39,40}

extrapolated critical scattering parameter, obtained using $\Delta\rho_0 = 30 \mu\Omega \text{ cm}$ and $\lambda = 260 \text{ nm}$, is $g_{exp}^\lambda \approx 3.7$. This value is much larger than that expected in the s^\pm scenario, quantifying the break-down of the AG theory in irradiated iron-arsenide superconductors, where the approximation of the uniformly impurity-averaged Green's function is not valid. Similar results were reported in Ba(Fe_{1-x}Co_x)₂As₂ irradiated by protons¹¹ and illustrate the generality of the Swiss cheese model for pair-breaking in this large class of high-temperature superconductors.

V. CONCLUSION

We reported the influence of random point disorder produced by proton irradiation on the superfluid density in Ca_{0.5}Na_{0.5}Fe₂As₂. It leads to a dramatic change of $\lambda(0)$ after irradiation, in contrast to the small variation of T_c and predictions by the AG theory. Both $\xi(T)$ and $\lambda(T)$ show similar temperature behavior before and after irradiation. This behavior may be understood within the Swiss cheese model, the pair-breaking nature of s^\pm inter-band superconductivity, and a short coherence length, which considers the spatial dependence of the order parameter and its strong suppression near defects at the atomic scale. Finally, the extracted normalized scattering rate, in conjunction with the absolute value of $\lambda(T)$, is much larger than the critical scattering rate for the s^\pm pairing, confirming the break-down of the AG theory in these disordered superconductors. Further detailed multiband BdG model calculations combined with systematic doping and irradiation studies may shed light on the suppression of superconductivity in this large class of iron-based superconductors.

Work at LANL was supported by the US Department of Energy, Basic Energy Sciences, Division of Materials Sciences and Engineering. Work at Brookhaven was supported by the US Department of Energy under Contract No. DE-AC02-98CH10886. Work by G.F.C. and W.Y. (fabrication of samples) was supported by the NSFC under Grants No. 10974254 and No. 11074304, and by the National Basic Research Program of China under Grants No. 2010CB923000 and No. 2011CBA00100. N.H. is member of CONICET (Argentina).

* Corresponding author: jeehoon@lanl.gov

¹ K. Hashimoto, T. Shibauchi, S. Kasahara, K. Ikada, S. Tonegawa, T. Kato, R. Okazaki, C. J. van der Beek, M. Konczykowski, H. Takeya, K. Hirata, T. Terashima, and Y. Matsuda, Phys. Rev. Lett. **102**, 207001 (2009).

² K. Ishida, Y. Nakai, and H. Hosono, J. Phys. Soc. Jpn. **78**, 062001 (2009).

³ C. Martin, R. T. Gordon, M. A. Tanatar, H. Kim, N. Ni, S. L. Bud'ko, P. C. Canfield, H. Luo, H. H. Wen, Z. Wang, A. B. Vorontsov, V. G. Kogan, and R. Prozorov, Phys. Rev. B **80**, 020501(R) (2009).

⁴ M. A. Tanatar, J.-Ph. Reid, H. Shakeripour, X. G. Luo, N. Doiron-Leyraud, N. Ni, S. L. Bud'ko, P. C. Canfield, R. Prozorov, and Louis Taillefer, Phys. Rev. Lett. **104**, 067002 (2010).

⁵ Kazuhiko Kuroki, Seiichiro Onari, Ryotaro Arita, Hidetomo Usui, Yukio Tanaka, Hiroshi Kontani, and Hideo Aoki, Phys. Rev. Lett. **101**, 087004 (2008); Kazuhiko Kuroki, Seiichiro Onari, Ryotaro Arita, Hidetomo Usui, Yukio Tanaka, Hiroshi Kontani, and Hideo Aoki, Phys. Rev. Lett. **102**, 109902(E) (2009).

⁶ K. Nakayama, T. Sato, P. Richard, Y.-M. Xu, Y. Sekiba, S. Souma, G. F. Chen, J. L. Luo, N. L. Wang, H. Ding and T. Takahashi, EPL **85**, 67002 (2009).

⁷ I. I. Mazin, D. J. Singh, M. D. Johannes, and M. H. Du, Phys. Rev. Lett. **101**, 057003 (2008).

⁸ P. W. Anderson, Phys. Rev. Lett. **3**, 325 (1959); T. Tsuneto, Prog. Theor. Phys. **28**, 857 (1962); D. Markowitz and L.P. Kadanoff, Phys. Rev. **181**, 563 (1963).

⁹ C.J. Pethick and D. Pines, Phys. Rev. Lett. **57**, 118 (1986); S. Schmitt-Rink, K. Miyake, and C.M. Varma, ibid. **57**, 2575 (1986); P.J. Hirschfeld, P. Wolfe, and D. Einzel, Phys. Rev. B **37**, 83 (1988).

¹⁰ James Annett, Nigel Goldenfeld, and S. R. Renn, Phys. Rev. B **43**, 2778 (1991).

¹¹ H. Kim, R. T. Gordon, M. A. Tanatar, J. Hua, U. Welp, W. K. Kwok, N. Ni, S. L. Budko, P. C. Canfield, A. B. Vorontsov, and R. Prozorov, Phys. Rev. B **82**, 060518(R) (2010).

¹² Y. Nakajima, T. Taen, Y. Tsuchiya, T. Tamegai, H. Kitamura, and T. Murakami, Phys. Rev. B **82**, 220504 (2010).

¹³ A. A. Abrikosov and L. P. Gorkov, Zh. Éksp. Teor. Fiz.

- 39**, 1781 (1960) [Sov. Phys. JETP **12**, 1243 (1961)].
- ¹⁴ J. M. Byers, M. E. Flatte, and D. J. Scalapino, Phys. Rev. Lett. **71**, 3363 (1993).
 - ¹⁵ A. V. Balatsky, M. I. Salkola, and A. Rosengren, Phys. Rev. B **51**, 15547 (1995).
 - ¹⁶ M. E. Flatté and J. M. Byers, Phys. Rev. Lett. **78**, 3761 (1997).
 - ¹⁷ M. I. Salkola, A. V. Balatsky, and J. R. Schrieffer, Phys. Rev. B **55**, 12648 (1997).
 - ¹⁸ M. H. Hettler and P. J. Hirschfeld, Phys. Rev. B **59**, 9606 (1999).
 - ¹⁹ Jian-Xin Zhu, T. K. Lee, C. S. Ting, and C.-R. Hu, Phys. Rev. B **61**, 8667 (2000).
 - ²⁰ A. V. Balatsky, I. Vekhter, and Jian-Xin Zhu, Rev. Mod. Phys. **78**, 373 (2006).
 - ²¹ Y. Bang, EPL **86**, 47001 (2009).
 - ²² A. B. Vorontsov, M. G. Vavilov, and A. V. Chubukov, Phys. Rev. B **79**, 140507 (2009).
 - ²³ R. T. Gordon, H. Kim, M. A. Tanatar, R. Prozorov, and V. G. Kogan, Phys. Rev. B **81**, 180501(R) (2010).
 - ²⁴ J. Kim, F. Ronning, N. Haberkorn, L. Civale, E. Nazaretski, N. Ni, R. J. Cava, J. D. Thompson, and R. Movshovich, Phys. Rev. B **85**, 180504(R) (2012).
 - ²⁵ J. Kim, L. Civale, E. Nazaretski, N. Haberkorn, F. Ronning, A. S. Sefat, T. Tajima, B. H. Moeckly, J. D. Thompson, R. Movshovich, e-print arXiv:1206.4525.
 - ²⁶ J. Kim, N. Haberkorn, S.-Z. Lin, L. Civale, E. Nazaretski, B. H. Moeckly, C. S. Yung, J. D. Thompson, R. Movshovich, Phys. Rev. B **86**, 024501 (2012).
 - ²⁷ J. H. Xu, J. H. Miller, Jr., and C. S. Ting, Phys. Rev. B **51**, 424 (1995).
 - ²⁸ M. W. Coffey, Phys. Rev. B **52**, R9851 (1995).
 - ²⁹ N. Haberkorn, B. Maierov, M. Jaime, I. Usov, M. Miura, G. F. Chen, W. Yu, and L. Civale, Phys. Rev. B **84**, 064533 (2011).
 - ³⁰ L. Civale *et al.*, Phys. Rev. Lett. **65**, 1164 (1990).
 - ³¹ N. Haberkorn, B. Maierov, I. O. Usov, M. Weigand, W. Hirata, S. Miyasaka, S. Tajima, N. Chikumoto, K. Tanabe, and Leonardo Civale, Phys. Rev. B **85**, 014522 (2012).
 - ³² E. Nazaretski, K. S. Graham, J. D. Thompson, J. A. Wright, D. V. Pelekhov, P. C. Hammel, and R. Movshovich, Rev. Sci. Instrum. **80**, 083704 (2009).
 - ³³ C. Martin *et al.*, Phys. Rev. Lett. **102**, 247002 (2009).
 - ³⁴ A SSS-QMFM cantilever, Nanosensors, Inc.
 - ³⁵ E. D. Bauer *et al.*, J. Alloys Compd. **488**, 554 (2009).
 - ³⁶ Y. J. Uemura *et al.*, Phys. Rev. Lett. **62**, 2317 (1989).
 - ³⁷ T. Das, J. X. Zhu, and M. J. Graf, Phys. Rev. B **84**, 134510 (2011).
 - ³⁸ K. Ohishi *et al.*, Phys. Rev. B **76**, 064504 (2007).
 - ³⁹ D. N. Basov, A. V. Puchkov, R. A. Hughes, T. Strach, J. Preston, T. Timusk, D. A. Bonn, R. Liang, and W. N. Hardy, Phys. Rev. B **49**, 12165 (1994).
 - ⁴⁰ S. H. Moffat, R. A. Hughes, and J. S. Preston, Phys. Rev. B **55**, R14741 (1997).
 - ⁴¹ M. Franz, C. Kallin, A. J. Berlinsky, and M. I. Salkola, Phys. Rev. B **56**, 7882 (1997).
 - ⁴² Z. Szotek, B. L. Gyorffy, and W. M. Temmerman, Phys. Rev. B **62**, 3997 (2000).
 - ⁴³ M. Prohammer and J. P. Carbotte, Phys. Rev. B **43**, 5370 (1991).
 - ⁴⁴ H. Kim, G. Preosti, and P. Muzikar, Phys. Rev. B **49**, 3544 (1994).
 - ⁴⁵ A. V. Chubukov, D. V. Efremov, and I. Eremin, Phys. Rev. B **78**, 134512 (2008).